Coherent control of resonant two-photon transitions by counterpropagating ultrashort pulse pairs

Woojun Lee, Hyosub Kim, Kyungtae Kim, and Jaewook Ahn*
Department of Physics, KAIST, Daejeon 305-701, Korea
(Received 10 March 2015; published 14 September 2015)

We describe optimized coherent control methods for two-photon transitions in atoms of a ladder-type three-state energy configuration. Our approach is based on the spatial coherent control scheme, which uses counterpropagating ultrashort laser pulses to produce complex excitation patterns in an extended space. Because coherent control requires constructive interference of constituent transition pathways, applying it to an atomic transition with a specific energy configuration requires specially designed laser pulses. We show in an experimental demonstration that two-photon transition with an intermediate resonant energy state can be coherently controlled and retrieved from the resonance-induced background, when phase flipping of the laser spectrum near the resonant intermediate transition is used. A simple reason for this behavior is the fact that the transition amplitude function (added to give an overall two-photon transition) changes its sign at the intermediate resonant frequency and, thus, by proper spectral-phase programing, the excitation patterns (or the position-dependent interference of the transition given as a consequence of the spatial coherent control) can be well isolated in space along the focal region of the counterpropagating pulses.

DOI: 10.1103/PhysRevA.92.033415 PACS number(s): 32.80.Qk, 78.47.jh, 42.65.Re

I. INTRODUCTION

Femtosecond laser optics have been widely used over the last two decades as a time-resolving spectroscopic means of studying the ultrafast time-scale dynamics of a variety of quantum systems, including atoms, molecules, and quasiparticles in solids [1–5]. The extreme peak intensity of femtosecond laser pulses has also enabled high-order nonlinear optical processes such as multiphoton excitations, high-harmonic generations, and above-threshold ionizations, to list a few [6–9]. Besides these uses, femtosecond lasers have gradually become an important tool in the field of coherent control [10–12], where shaped laser pulses steer quantum processes towards certain desirable outcomes. The information of as-obtained laser pulse shapes through coherent control often plays a crucial role in understanding the quantum structure of the materials under consideration [13–16]. In this regard, researchers can furthermore analytically design the optimized laser pulse shapes for more selective and efficient nonlinear optical processes [17–23].

The recent demonstration [24] of a counterpropagating pair of ultrafast laser pulses coherently inducing Doppler-free two-photon transitions of atoms shows the intriguing possibility for its use in ultraprecision spectroscopy [25], especially in conjunction with a femtosecond frequency comb [26,27]. This method, termed spatial coherent control, coherently arranges in time the spectral components of the laser pulse in such a way that all of the counterpropagating photon pairs, energy resonant to the atomic transition (i.e., $\hbar\omega_1 + \hbar\omega_2 = E_e - E_g$), collide only at specific locations along the beam direction. Because the resonance condition varies from one atomic species to another, the atom-specific spectroscopic information can be retrieved by imaging the distinct spatial excitation profile if a proper coherent control scheme is used. So far, this powerful method of spatial coherent control has been demonstrated for nonresonant two-photon transitions (or for cases in which intermediate states are not directly involved with the transition) and not yet demonstrated for resonant two-photon transitions (two-photon transitions with a resonant intermediate state or states).

In this paper, we describe an experimental demonstration of the spatial coherent control of the *resonant two-photon transition* $5S_{1/2} \rightarrow 5P_{2/3} \rightarrow 5D$ of atomic rubidium (^{85}Rb). Ultrashort laser pulses are programed in such a way that not only (1) counterpropagating photon pairs, and no photon pairs in the same propagation direction, induce the given transition, but also (2) the contributions from all possible combinations of photon energies involving such transition are coherently added for an optimal net transition probability. To accomplish this, we first adopt spectral pulse-shaping methods: V-shaped spectral phase programming for condition (1) and a spectral step phase for condition (2) in the first and second experiments. On the basis of the single-pulse-based pulse-shaping method [17,23], we resolve the issue of the resonant intermediate transition and extend the method in the context of the spatial excitation pattern formation by counterpropagating pulses. In the subsequent experiment, we use additionally a spectral amplitude shaping method to further enhance the net two-photon transition, in which the resonant intermediate transition is spectrally blocked so that the spatially extended excitation caused by sequential two-photon transitions through the intermediate resonant state is completely avoided.

In the remaining sections, we first theoretically sketch the laser-pulse-shaping ideas relevant for the resonant and nonresonant two-photon transitions, respectively, in Sec. II, before the experimental procedure is described in Sec. III. We then present the experimental results of the spatial coherent control of the two-photon transition of ^{85}Rb in Sec. IV and our conclusions in Sec. V.

*jwahn@kaist.ac.kr

II. THEORETICAL CONSIDERATIONS

We consider a pair of laser pulses, denoted by $\mathcal{E}_1(z,t)$ and $\mathcal{E}_2(z,t)$, respectively propagating along the $\pm z$ directions interacting with a three-state atom in a ladder-type energy configuration. The dynamics of the three-state system is governed by the Schrödinger equation, which reads

$$i\hbar\frac{d\mathbf{c}(t)}{dt} = H(t)\mathbf{c}(t), \tag{1}$$

where $\mathbf{c} = [c_g(t), c_i(t), c_e(t)]^T$ is the column vector with the probability amplitudes $c_g(t)$, $c_i(t)$, and $c_e(t)$ of the three states: $|\psi_g\rangle$ (the ground state), $|\psi_i\rangle$ (the intermediate state), and $|\psi_e\rangle$ (the final state). In the perturbative interaction regime, the two-photon transition amplitude $c_e(t)$ is then obtained from the second-order Dyson series as

$$c_e(z,t) = -\frac{\mu_{ei}\mu_{ig}}{2\pi\hbar^2}\int_{-\infty}^{t} dt_1 e^{i\omega_{ei}t_1}\mathcal{E}(z,t_1) \times \int_{-\infty}^{t_1} dt_2 e^{i\omega_{ig}t_2}\mathcal{E}(z,t_2), \tag{2}$$

where $\mathcal{E}(z,t) = \mathcal{E}_1(z,t) + \mathcal{E}_2(z,t)$ and μ_{ei} and μ_{ig} are the corresponding dipole moments of the atom. The integration provides the transition probability amplitude c_e in terms of the spectral amplitudes (including phase) $E_1(\omega) = f[\mathcal{E}_1(0,t)]$ and $E_2(\omega) = f[\mathcal{E}_2(0,t)]$ by

$$c_e(z) = i\frac{\mu_{ei}\mu_{ig}}{\hbar^2}\left[i\pi E(\omega_{ig})E(\omega_{ei}) + \int_{-\infty}^{\infty}\frac{E(\omega)E(\omega_{eg}-\omega)}{\omega_{ig}-\omega}\right], \tag{3}$$

where $E(\omega) = E_1(\omega)e^{-i\omega z/c} + E_2(\omega)e^{i\omega z/c}$ and $t \to \infty$ is assumed. We denote the first term in the bracket of Eq. (3) by $c_r(z)$, the resonant two-photon transition, and the second term by $c_{nr}(z)$, the nonresonant two-photon transition, i.e.,

$$c_e(z) = c_r(z) + c_{nr}(z), \tag{4}$$

which can be respectively written in terms of $E_1(\omega)$ and $E_2(\omega)$ as

$$c_r(z) = -\pi\frac{\mu_{ei}\mu_{ig}}{\hbar^2}[E_1(\omega_{ig})E_1(\omega_{ei}) + E_2(\omega_{ig})E_2(\omega_{ei})e^{2i\omega_{eg}z/c} + E_1(\omega_{ig})E_2(\omega_{ei})e^{2i\omega_{ei}z/c} + E_2(\omega_{ig})E_1(\omega_{ei})e^{2i\omega_{ig}z/c}], \tag{5}$$

$$c_{nr}(z) = i\frac{\mu_{ei}\mu_{ig}}{\hbar^2}\int_{-\infty}^{\infty}\frac{d\omega}{\omega_{ig}-\omega} \times [E_1(\omega)E_1(\omega_{eg}-\omega) + E_2(\omega)E_2(\omega_{eg}-\omega)e^{2i\omega_{eg}z/c} + E_1(\omega)E_2(\omega_{eg}-\omega)e^{2i(\omega_{eg}-\omega)z/c} + E_2(\omega)E_1(\omega_{eg}-\omega)e^{2i\omega z/c}], \tag{6}$$

where the global phase factor $\exp(-i\omega_{eg}z/c)$ was omitted in both equations and the two-photon resonance condition is given by $\omega_{eg} = \omega_{ei} + \omega_{ig}$.

Note that the first two terms in each bracket in Eqs. (5) and (6) are the single-pulse contributions from either direction of the pulse propagations while the last two terms are caused by the counterpropagation of the pulses. The phase factors of the last two terms in $c_{nr}(z)$ have both ω and z dependence and, thus, are involved in the integration over ω, generating a nontrivial macroscopic spatial two-photon excitation profile which can be programed via spectral phase modulation. The other terms have only rapidly oscillating or constant phase factors, making no contribution to the macroscopic spatial profile. With the last two terms of $c_{nr}(z)$, the spatial excitation probability is given by, proportionally,

$$S(z) \propto \left|\int_{-\infty}^{\infty} d\omega\frac{A(\omega)A(\omega_{eg}-\omega)}{\omega_{ig}-\omega}e^{i[\Phi(\omega)+\Phi(\omega_{eg}-\omega)]} \times [e^{2i\omega z/c} + e^{2i(\omega_{eg}-\omega)z/c}]\right|^2, \tag{7}$$

where the spectral amplitude function $A(\omega)$ and the spectral phase function $\Phi(\omega)$ are defined the same for both pulses, when they are split from a single laser pulse, as

$$E_1(\omega) = E_2(\omega) = A(\omega)e^{i\Phi(\omega)}. \tag{8}$$

A. Two-photon transition without a resonant intermediate state

First we consider the *nonresonant two-photon transition* case, in which the one-photon transition to the intermediate state $|\psi_i\rangle$ is out of the laser spectrum (i.e., $\omega_{ig} < \omega_{\min}$). In this case, we can ignore the sign change of the denominator $\omega_{ig} - \omega$ in Eq. (7) across the laser spectrum ω_{ig} in the context of spatial coherent control, and the phase function $\Phi(\omega)$ can be programed in such a way that the two-photon transition components in the integral calculation in Eq. (7) satisfy a constructive interference condition only at specific positions. For example, with a spectral phase such as

$$\Phi_V(\omega) = \alpha|\omega - \omega_o|, \tag{9}$$

called a V-shaped spectral phase, where ω_o denotes the two-photon center ($\omega_o = \omega_{eg}/2$), each of the position-dependent oscillating phase terms in the integrand in Eq. (7) is canceled out at the points $z = \pm z_o$, where $z_o = \alpha c$. Because $\omega < \omega_0$ and $\omega > \omega_0$ parts of the modulated phase term have opposite slopes, the V-shaped phase in Eq. (9) divides a pulse in the time domain into two subpulses, each of which has a group delay of $-\alpha$ for the $\omega > \omega_0$ part and of α for the $\omega < \omega_0$ part, from the group delay relation $\alpha = -|d\Phi_V/d\omega|$. So, a pair of counterpropagating pulses with these subpulses makes two distinct local excitations at the points where a red subpulse and a blue subpulse meet up to fulfill the two-photon transition condition. The spatial excitation profile $S(z)$ in Eq. (7) is, therefore, conceptually given in this case by

$$S(z) \propto \delta(z - z_o) + \delta(z + z_o), \tag{10}$$

where $\delta(z)$ is a Dirac delta function. Figure 1 compares the numerically calculated spatial excitation patterns for various phase programing. As shown in Figs. 1(a) and 1(b), the V-shaped spectral phase, $\Phi_V(\omega)$, causes local excitations to occur at points $z = \pm z_o$ in nonresonant two-photon transitions [25].

B. Two-photon transitions with a resonant intermediate state

However, in the *resonant two-photon transition* case, in which the intermediate state is located within the laser spectrum (i.e., $\omega_{\min} < \omega_{ig} < \omega_{\max}$), we need alternative phase

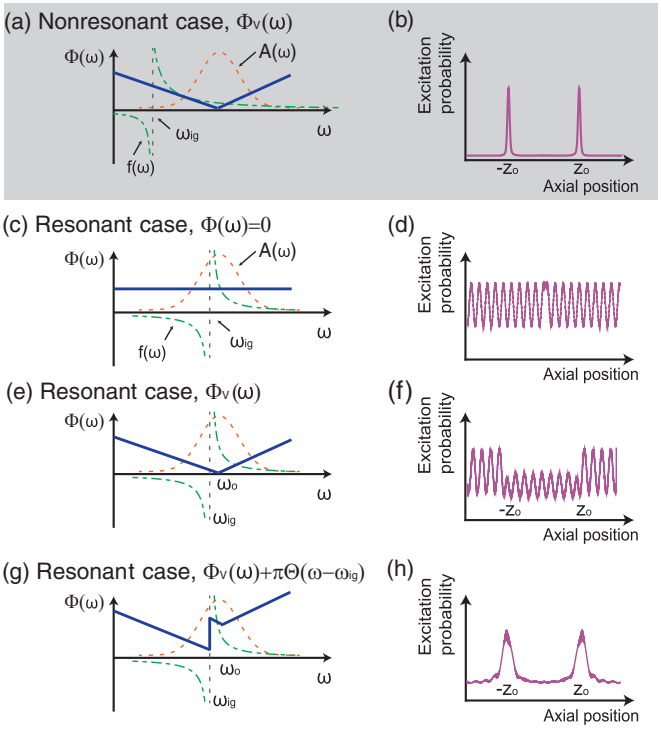

FIG. 1. (Color online) Spectral phase function $\Phi(\omega)$ vs the excitation probability $|c_e|^2$ calculated from Eq. (7) for (a, b) the nonresonant two-photon transition case with $\Phi_V(\omega)$ and (c–h) the resonant two-photon transition cases with (c, d) $\Phi(\omega) = 0$, (e, f) $\Phi_V(\omega)$, and (g, h) $\Phi_V(\omega) + \pi\Theta(\omega - \omega_{ig})$. The spectral amplitude $A(\omega)$ (orange dotted line) and the dispersion $f(\omega) = 1/(\omega - \omega_{ig})$ (green dash-dotted line) are plotted in comparison.

function programing to deal with the sign change of the denominator $\omega_{ig} - \omega$ in Eq. (7). When the position dependence is ignored, it is known that, by flipping the phase of either part of $\omega < \omega_{ig}$ or $\omega > \omega_{ig}$, the integrand becomes in-phase across ω_{ig}, resulting in an enhancement of the two-photon transition [17,23]. This phase flipping can be achieved with step-phase modulation such as $\pi\Theta(\omega - \omega_{ig})$, where $\Theta(x)$ denotes the Heaviside step function. If we combine this step-phase modulation with the V-shaped spectral phase in Eq. (9), the phase modulation is given by

$$\Phi(\omega) = \Phi_V(\omega) + \pi\Theta(\omega - \omega_{ig}), \tag{11}$$

and with this expression, Eq. (7) becomes

$$S(z) \propto \left| \int_{-\infty}^{\infty} d\omega \frac{A(\omega)A(\omega_{eg} - \omega)}{|\omega_{ig} - \omega|} e^{2i\Phi_V(\omega)} \times [e^{2i\omega z/c} + e^{2i(\omega_{eg}-\omega)z/c}] \right|^2, \tag{12}$$

when we ignore the small contribution from the spectral tail part ($\omega > \omega_{ei}$) of the laser spectrum. This expression has both a transition enhancement part, which is achieved by the step phase $\pi\Theta(\omega - \omega_{ig})$, and a spatial excitation part, which contains $\Phi_V(\omega) = \alpha|\omega - \omega_0|$, in its integrand. Figure 1 shows the numerical calculation of Eq. (7) for three cases: $\Phi(\omega) = 0$ [Figs. 1(c) and 1(d)], $\Phi_V(\omega)$ [Figs. 1(e) and 1(f)], and $\Phi_V(\omega) + \pi\Theta(\omega - \omega_{ig})$ [Figs. 1(g) and 1(h)]. As

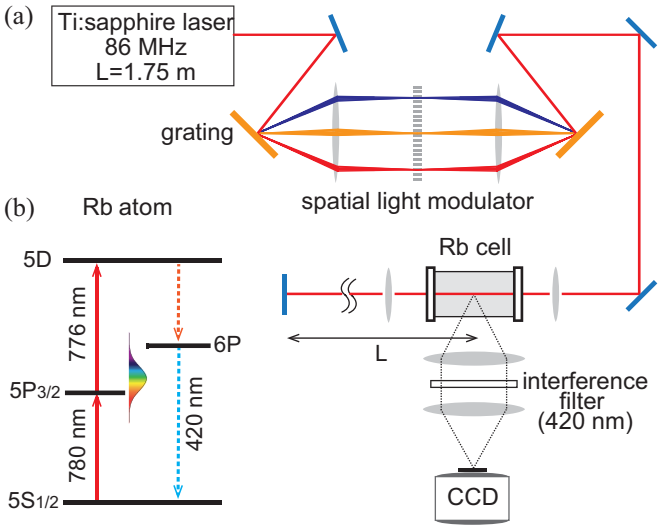

FIG. 2. (Color online) (a) Schematic diagram of the experimental setup. Ultrafast laser pulses were programed by a spatial light modulator to interact with rubidium atoms in a colliding pulse geometry. The cavity length $L = 1.75$ m of the laser was matched with the extra travel of the reflected pulses. (b) The energy-level diagram of atomic rubidium. Atoms are excited from $5S_{1/2}$ to $5D$ and decayed to $6P$. The fluorescence from $6P$ was monitored.

clearly shown in Fig. 1(h), the phase-modulation scheme of Eq. (11) in a counterpropagating pulse excitation is expected to induce a clear spatial excitation pattern of resonant two-photon transitions.

III. EXPERIMENTAL PROCEDURES

The experimental setup is schematically shown in Fig. 2(a). Femtosecond optical pulses were generated from a conventional Ti:sapphire laser oscillator (with a cavity length $L = 1.75$ m) mode locked around the center frequency set to the two-photon transition frequency (i.e., $\omega_o = \omega_{eg}/2$). The laser bandwidth (full width at half maximum) was 25 nm in wavelength scale. The pulses were then spectrally resolved in a $4f$-geometry Fourier plane and phase-modulated by a 128-pixel spatial-light modulator (SLM) [28] to program $\Phi(\omega)$. The focal length of the $4f$ geometry was 200 mm and the groove density of both gratings was 1200 mm^{-1} [29]. The width of each pixel in the SLM was 100 μm and the pulse bandwidth incident into each pixel was 0.37 nm in wavelength scale. After pulse shaping, the pulses were focused in a rubidium vapor cell (^{85}Rb) located at $z = 0$, defocused, collimated, and then reflected back by a mirror located at $z = L$, so that each counterpropagating laser pulse collided with the next pulse in the vapor cell. The focal length of both focusing lenses was 200 mm. The beam diameter and the Rayleigh range of the focus were approximately 50 μm and 2.5 mm, respectively.

The ^{85}Rb atoms were two-photon excited from the ground state $|g\rangle = 5S_{1/2}$ to the final state $|e\rangle = 5D$ via the intermediate state $|i\rangle = 5P_{3/2}$ [see Fig. 2(b)]. The corresponding frequencies (wavelengths) were $\omega_{ig}/2\pi = 384.6$ THz ($\lambda_{ig} = 780$ nm), $\omega_{ei}/2\pi = 386.6$ THz ($\lambda_{ei} = 776$ nm), and $\omega_o/2\pi = 385.6$ THz ($\lambda_o = 778$ nm), respectively [30]. Note that the D_1

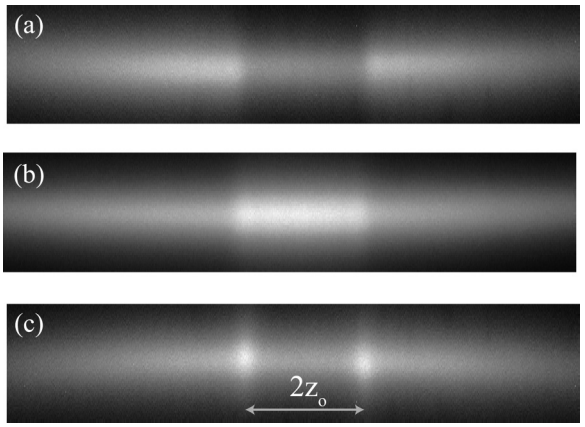

FIG. 3. Photo images of the fluorescence signals: (a, b) V-shaped spectral phase functions $\Phi_V(\omega)$ are used respectively with (a) $\alpha = -1.4$ ps and (b) $\alpha = +1.4$ ps. (c) The spectral phase function with a phase step, $\Phi(\omega)$ with $\alpha = -1.4$ ps. [$\Phi_V(\omega)$ and $\Phi(\omega)$ are defined in Eqs. (9) and (11), respectively, and $z_o = 420$ μm in (c).]

transition to the $5P_{1/2}$ state was out of the laser spectral range. The excited atoms in the $5D$ first decayed to $6P$, and then the spatial profile of the fluorescence at 420 nm ($6P \rightarrow 5S_{1/2}$) was imaged by a charge-coupled device (CCD) camera through one-to-one telescope imaging by a pair of $f = 25$ mm lenses. The image resolution of the camera was 4.54 μm.

IV. RESULTS AND DISCUSSION

The fluorescence images of position-independent background excitation in the resonant two-photon transition case described in Sec. II, with a dark or bright region in the center, were captured by a CCD camera and are shown in Figs. 3(a) and 3(b). In the resonant two-photon transition case, there occurs a position-independent background excitation in most of the region, which is caused by the excitation from the population remaining in the intermediate state $|i\rangle$ and which does not require the two different colors of subpulses simultaneously. Note that a dark region appears in $z < |z_o|$ for $\alpha < 0$ in Fig. 3(a) because the $|g\rangle \rightarrow |i\rangle$ excitation occurs later in time than $|i\rangle \rightarrow |e\rangle$. When $\alpha > 0$ in Fig. 3(b), however, a brighter region appears in $z < |z_o|$ for the same reason but with opposite causality. In spite of this aspect, we show that spatial excitation appears in the resonant two-photon transition case, with the phase-flipping step function modulation described earlier. The retrieval of spatial excitation achieved by phase-flipping modulation in Eq. (11) is shown in Fig. 3(c).

Figure 4 shows the result of the experiment performed with the spectral phase function described in Eq. (11), with varying step height, as

$$\Phi(\omega) = \alpha|\omega - \omega_0| + \beta\Theta(\omega - \omega_{ig}), \tag{13}$$

in comparison with a corresponding numerical calculation of the spatial excitation probability, from Eqs. (5) and (6). By maintaining the phase-slope value fixed at $\alpha = -1.0$ ps, the phase-step value was changed from $\beta = 0$ to 2π, and the fluorescence signals (measured on the line profile along the z direction where the position is shown in the horizontal axis) were plotted as a function of β (along the vertical axis) in

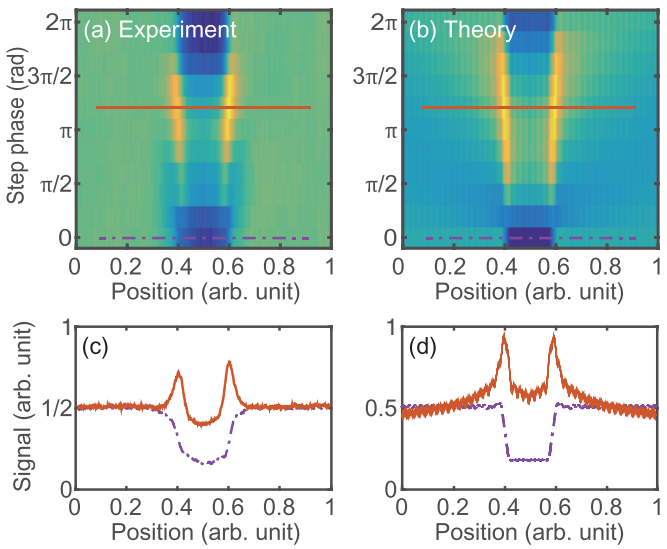

FIG. 4. (Color online) The phase-only modulation experiment: (a, c) spatial fluorescence signals for $\Phi(\omega)$ (V-shaped + phase step) spectral functions with $\alpha = -1.0$ ps and (b, d) the numerical simulation. Signals at $\beta = 0$ (purple dash-dotted line) and 1.2π (red solid line) are extracted from (a) and (b) and shown in (c) and (d), respectively.

Fig. 4(a). As expected, sharp fluorescence peaks appear at $z = \pm z_o$, when β is around π. The spatial excitation profiles measured at $\beta = 0$ (purple dash-dotted line) and 1.2π (red solid line) are respectively shown in Fig. 4(c). This experimental result agrees well with the numerical simulation as shown in Figs. 4(b) and 4(d). Here, one-photon-resonant background signals that were position insensitive were subtracted for clarity by means of numerical fitting with the focal spot profiles of counterpropagating Gaussian beams.

The behavior that the maximum peak signal in Fig. 4 exhibits at $\beta = 1.2\pi$, rather than at $\beta = \pi$, is due to the presence of the resonant amplitude term $c_r(z)$ in Eq. (5). If we divide the nonresonant term $c_{nr}(z)$ in Eq. (6) into c_{nr}^+ and c_{nr}^-, where c_{nr}^+ and c_{nr}^- denote the positive and negative parts of $c_{nr}(z)$ integrated for $\omega > \omega_{ig}$ and $\omega < \omega_{ig}$, respectively, the c_{nr}^+ term is 90° phase advanced and the c_{nr}^- term is 90° phase delayed with respect to the c_r term. Figure 5 graphically depicts c_r, c_{nr}^+, and c_{nr}^- on the complex plane, where Fig. 5(a) corresponds to the case in which c_{nr}^+ rotates by the applied step phase and the others remain unchanged. To ensure that the amplitude of the vector sum of all of the vectors reaches

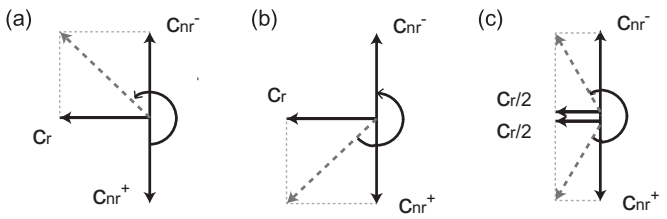

FIG. 5. Transition amplitude change graphically depicted on the complex plane when (a) c_{nr}^+, (b) $c_{nr}^+ + c_r$, and (c) $c_{nr}^+ + c_r/2$ are phase rotated, respectively.

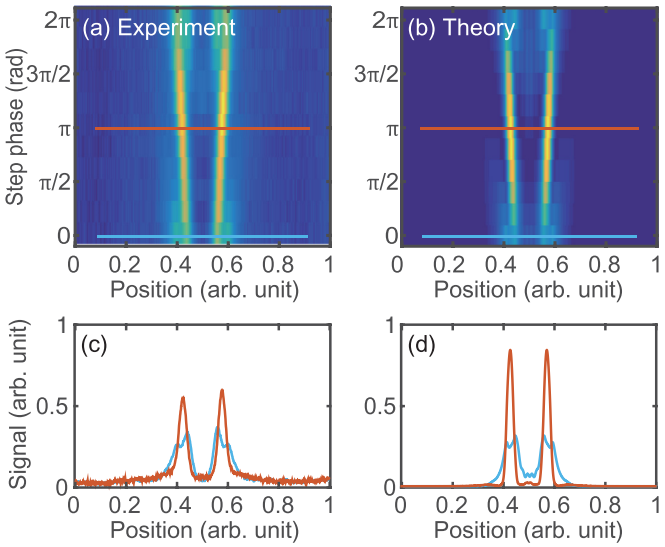

FIG. 6. (Color online) The phase and amplitude modulation experiment: (a, c) spatial fluorescence signals for $\Phi(\omega)$ (V-shaped + phase step) spectral functions with $\alpha = -1.0$ ps and (b, d) the numerical simulation. Signals at $\beta = 0$ (light blue line) and π (red line) are extracted from (a) and (b) and shown in (c) and (d), respectively.

the maximum, the phase rotation angle has to be greater than π and smaller than 1.5π. This explains the step phase of 1.2π for the maximum peak. A similar explanation applies to the case in Fig. 5(b) in which c_r and c_{nr}^{+} rotate together. Figure 5(c) gives a more realistic description in which c_r partially rotates along with c_{nr}^{+} due to the fact that the size of the focal spot passing through the spatial light modulator is finite, and provides the same conclusion.

In addition to the spectral phase modulation, we also tested *spectral amplitude modulation*, where the spectral components near the intermediate resonant transition ω_{ig} were removed. In this case, we only have the nonresonant contribution $c_{nr}(z)$ but not the resonant contribution $c_r(z)$. For this, the resonant spectrum was blocked with a 120-μm-wide copper wire placed in the Fourier plane, which corresponds to 0.44 nm in wavelength. In this circumstance, the resonant transition from the $5S_{1/2}$ state to the $5P_{3/2}$ state is suppressed, so excitations only occur at the points where the two photons with frequencies ω_{ig} and $\omega_{eg} - \omega_{ig}$, respectively, collide with each other. The phase modulation of Eq. (13) from the first experiment was again applied, with $\alpha = -1.0$ ps. As shown in Figs. 6(a) and 6(c), the phase modulation with $\beta = \pi$ (red line) enhances and more tightly localizes the peaks than the bare V-shaped phase does (light blue line). This result again compares with the theoretical prediction in Figs. 6(b) and 6(d). The maximal peak appears at $\beta = \pi$ because of the complete removal of the resonant amplitude term.

V. CONCLUSION

In summary, we performed coherent control experiments with counterpropagating phase-modulated ultrashort pulses for the two-photon excitations in the ladder-type three-state quantum system of atomic rubidium. The laser pulses, designed on the basis of the spatial coherent control scheme to phase-flip the laser spectrum near the resonant intermediate transition, successfully produced spatially localized excitation patterns from the resonance-induced background along the focal region of the counterpropagating pulses. The resulting constructive interference phenomena among the constituent nonresonant two-photon transitions were theoretically confirmed and verified by numerical calculations. The presented scheme of coherent control has possible applications in Doppler-free frequency-comb spectroscopy of the resonant two-photon transitions. Since the phase flipping across a particular intermediate resonance provides a two-photon transition enhancement selectively through the given intermediate state, it is hoped that this phase-programing method will be useful for atom and resonance-specific laser spectroscopy.

ACKNOWLEDGMENTS

This research was supported by Samsung Science and Technology Foundation (Grant No. SSTF-BA1301-12). The experimental apparatus was constructed and in part supported by Basic Science Research Program (Grant No. 2013R1A2A2A05005187) through the National Research Foundation of Korea.

[1] P. Antoine, A. L'Huillier, and M. Lewenstein, Attosecond Pulse Trains Using High-Order Harmonics, Phys. Rev. Lett. **77**, 1234 (1996).

[2] A. H. Zewail, Femtochemistry: Atomic-scale dynamics of the chemical bond using ultrafast lasers (Nobel lecture), Angew. Chem. Int. Ed. Engl. **39**, 2587 (2000).

[3] J. Ahn, D. N. Hutchinson, C. Rangan, and P. H. Bucksbaum, Quantum Phase Retrieval of a Rydberg Wavepacket Using a Half-Cycle Pulse, Phys. Rev. Lett. **86**, 1179 (2001).

[4] G. C. Cho, W. Kutt, and H. Kurz, Subpicosecond Time-Resolved Coherent-Phonon Oscillations in GaAs, Phys. Rev. Lett. **65**, 764 (1990).

[5] T. K. Cheng, S. Vidal, M. J. Zeiger, G. Dresselhaus, M. S. Dresselhaus, and E. P. Ippen, Mechanism for displacive excitation of coherent phonons in Sb, Bi, Te, and Ti_2O_3, Appl. Phys. Lett. **59**, 1923 (1991).

[6] T. Brabec and F. Krausz, Intense few-cycle laser fields: Frontiers of nonlinear optics, Rev. Mod. Phys. **72**, 545 (2000).

[7] R. R. Freeman, P. H. Bucksbaum, H. Milchberg, S. Darack, D. Schumacher, and M. E. Geusic, Above-Threshold Ionization with Subpicosecond Laser Pulses, Phys. Rev. Lett. **59**, 1092 (1987).

[8] P. B. Corkum, Plasma Perspective on Strong-Field Multiphoton Ionization, Phys. Rev. Lett. **71**, 1994 (1993).

[9] P. Agostini and L. F. DiMauro, The physics of attosecond light pulses, Rep. Prog. Phys. **67**, 813 (2004).

[10] K. Bergmann, H. Theuer, and B. W. Shore, Coherent population transfer among quantum states of atoms and molecules, Rev. Mod. Phys. **70**, 1003 (1998).

[11] M. Shapiro and P. Brumer, *Principles of the Quantum Control of Molecular Processes* (Wiley, New York, 2003).

[12] D. J. Tanner and S. A. Rice, Control of selectivity of chemical reaction via control of wavepacket evolution, J. Chem. Phys. **83**, 5013 (1985).

[13] R. Bartels, S. Backus, E. Zeek, L. Misoguti, G. Vdovin, I. P. Christov, M. M. Murnane, and H. C. Kapteyn, Shaped-pulse optimization of coherent emission of high-harmonic soft X-rays, Nature (London) **406**, 164 (2000).

[14] J. L. Herek, W. Wohlleben, R. J. Cogdell, D. Zeidler, and M. Motzkus, Quantum control of energy flow in light harvesting, Nature (London) **417**, 533 (2002).

[15] J. M. Dela Cruz, I. Pastirk, M. Comstock, V. V. Lozovoy, and M. Dantus, Use of coherent control methods through scattering biological tissue to achieve functional imaging, Proc. Natl. Acad. Sci. USA **101**, 16996 (2004).

[16] V. I. Prokhorenko, A. M. Nagy, S. A. Waschuk, L. S. Brown, R. R. Birge, and R. J. Dwayne Miller, Coherent control of retinal isomerization in bacteriorhodopsin, Science **313**, 1257 (2006).

[17] N. Dudovich, B. Dayan, S. M. Gallagher Faeder, and Y. Silberberg, Transform-Limited Pulses are not Optimal for Resonant Multiphoton Transitions, Phys. Rev. Lett. **86**, 47 (2001).

[18] S. D. Clow, C. Trallero-Herrero, T. Bergeman, and T. Weinacht, Strong Field Multiphoton Inversion of a Three-Level System Using Shaped Ultrafast Laser Pulses, Phys. Rev. Lett. **100**, 233603 (2008).

[19] M. Reetz-Lamour, T. Amthor, J. Deiglmayr, and M. Weidemüller, Rabi Oscillations and Excitation Trapping in the Coherent Excitation of a Mesoscopic Frozen Rydberg Gas, Phys. Rev. Lett. **100**, 253001 (2008).

[20] S. Lee, J. Lim, C. Y. Park, and J. Ahn, Strong-field coherent control of 2+1 photon process in atomic sodium, Opt. Express **19**, 2266 (2011).

[21] J. Lim, H. G. Lee, J. U. Kim, S. Lee, and J. Ahn, Coherent transients mimicked by two-photon coherent control of three-level system, Phys. Rev. A **83**, 053429 (2011).

[22] J. Lim, H. G. Lee, S. Lee, and J. Ahn, Quantum control in two-dimensional Fourier transform spectroscopy, Phys. Rev. A **84**, 013425 (2011).

[23] H. G. Lee, H. Kim, J. Lim, and J. Ahn, Quantum interference control of four-level diamond-configuration quantum system, Phys. Rev. A **88**, 053427 (2013).

[24] I. Barmes, S. Witte, and K. S. E. Eikema, Spatial and spectral coherent control with frequency combs, Nat. Photonics **7**, 38 (2013).

[25] I. Barmes, S. Witte, and K. S. E. Eikema, High-Precision Spectroscopy with Counterpropagating Femtosecond Pulses, Phys. Rev. Lett. **111**, 023007 (2013).

[26] R. Holzwarth, Th. Udem, T. W. Hänsch, J. C. Knight, W. J. Wadsworth, and P. St. J. Russell, Optical Frequency Synthesizer for Precision Spectroscopy, Phys. Rev. Lett. **85**, 2264 (2000).

[27] D. J. Jones, S. A. Diddams, J. K. Ranka, A. Stentz, R. S. Windeler, J. L. Hall, and S. T. Cundiff, Carrier-envelope phase control of femtosecond mode-locked lasers and direct optical frequency synthesis, Science **288**, 635 (2000).

[28] A. M. Weiner, Femtosecond pulse shaping using spatial light modulators, Rev. Sci. Instrum. **71**, 1929 (2000).

[29] R. L. Fork, O. E. Martinez, and J. P. Gordon, Negative dispersion using pairs of prisms, Opt. Lett. **9**, 150 (1984).

[30] J. E. Sansonetti, Wavelengths, transition probabilities, and energy levels for the spectra of Rubidium (RbI through RbXXXVII), J. Phys. Chem. Ref. Data **35**, 301 (2006).